Noname manuscript No.
(will be inserted by the editor)

Fresnel phase retrieval method using an annular lens array on an SLM

V. Loriot[1,2⋆], O. Mendoza-Yero[3], J. Pérez Vizcaino[3], G. Mínguez-Vega[3], R. de Nalda[1], L. Bañares[2], J. Lancis Sáez[3]

[1] Instituto de Química Física Rocasolano, Consejo Superior de Investigaciones Científicas, 28006 Madrid, Spain, e-mail: vincent.loriot@univ-lyon1.fr
[2] Departamento de Química Física I (Unidad Asociada al CSIC), Facultad de Ciencias Químicas, Universidad Complutense de Madrid, 28040 Madrid, Spain
[3] GROC·UJI, Institut de Noves Tecnologies de la Imatge (INIT), Universitat Jaume I, 12080 Castelló, Spain

Received: date / Revised version: date

Abstract Wavefront aberrations play a major role when focusing an ultrashort laser pulse to a high quality focal spot. Here, we report a novel method to measure and correct wavefront aberrations of a 30 fs pulsed laser beam. The method only requires a programmable liquid crystal spatial light modulator and a camera. Wavefront retrieval is based on pupil segmentation with an annular lens array, which allows us to determine the local phase that minimizes focusing errors due to wavefront aberrations. Our method provides accurate results even when implemented with low dynamic range cameras and polychromatic beams. Finally, the retrieved phase is added to a diffractive lens codified onto the spatial light modulator to experimentally demonstrate near-diffraction-limited femtosecond beam focusing without refractive components.

Key words Diffractive optics – Ultrafast optics – Adaptive optics – Spatial light modulation

1 Introduction

Focusing ultrashort laser pulses to a small focal region is the key to a myriad of nonlinear optical phenomena such as nonlinear microscopic imaging, manipulation and machining. However, wavefront aberrations originated by imperfections, misalignments and stress of the optical mounts in the chains inside femtosecond amplifier systems enlarge the spatial dimensions of the focal spot. It is now well established that the measurement and the correction of wavefront aberrations of the laser pulse is crucial for high-quality stable focusing [1–3]. An adaptive optics system, which consists of a wavefront sensing device and a compensating unit, measures and corrects the wavefront aberrations of a laser pulse, and eventually delivers a near-diffraction-limited focal spot to a target. The above device has been successfully applied in such different fields as to generate high laser intensities in the range of 10^{22} W.cm^{-2} [4, 5], to increase the repetition rate of high-energy lasers [6] and to write optical waveguides in dielectric samples [7].

Accurate knowledge of the laser beam wavefront is the first step towards producing highly focused homogeneous intensity spots. Several phase-measurement methods have already been proposed and demonstrated. The most popular is the Shack-Hartmann wavefront sensor (SHWS) where the measurement of the local phase slopes of the wavefront provides the entire beam phase [1–7]. This technique requires a microlens array that divides the pulsed beam into a number of beamlets and has been implemented, for instance, to test the temporal stability of pulsed laser beams [8]. Achromatic lateral-shearing interferometers are particularly suited for the measurement of the wavefront of broadband ultrashort laser pulses because of their achromaticity [9]. Also, the angular and spectral dependences of second-harmonic generation conversion efficiency in uniaxial crystals have been used for phase measurement [10]. On the other hand, the Fresnel phase-retrieval method such as the early work of Fienup *et al.* [11] provides the spatial phase of the pulsed beam reconstructed from only two intensity distributions at two planes along the optical axis that are measured by means of simple CCD cameras. This technique has been successfully employed for terawatt-class femtosecond laser pulses with accuracy better than $\lambda/30$ peak to valley [12, 13]. The iterative Fourier transform algorithm is used to achieve an acceptable solution for the wavefront and the effects of the dynamic range of the sensor, the intensity noise, and the wavelength-dependent error in wavefront reconstruction are considered. Concerning wavelength error, the value was demonstrated to be negligible for long pulses of 100 fs but also

⋆ Present address: Institut Lumière Matière, UMR5306 Université Lyon 1-CNRS, Université de Lyon 69622 Villeurbanne cedex, France

claimed to increase proportionally with the bandwidth for shorter pulses.

On a completely different context, liquid-crystal displays working as electronically addressed spatial light modulators (SLM) have been widely used to generate programmable diffractive lenses (DL) to focus continuous wave laser radiation, either monochromatic [14] or polychromatic [15]. Also, arrays of lenses have been codified to implement a programmable SHWS [16]. Now, the mathematical models to optimize encoding of the lens function in a device constrained by the pixelated structure and the phase quantization of the SLM are well understood [17]. Although such lenses suffer from a relatively low pupil diameter and long focal length, they allow for an electronically controlled variable focal length. But, what is more important, the use of this kind of modulators introduces the benefit of local beam control of the phase of the lens which allows for minimizing focusing errors due to wavefront aberrations.

Here, we present a novel technique for wavefront retrieval of short pulses coming from commercial amplifier systems running at mJ energy levels and temporal pulse durations at tens of fs. The method requires the implementation of a DL onto the SLM, which is subsequently apertured through a set of concentric rings in a sequential way. Also, the intensity is measured with a camera at the focal plane for each ring-shaped zone. As a result, our technique is particularly well-fitted for the measurement of the drop of both the intensity profile and the diffraction efficiency at the outermost radial zones of the DL due to the reduced number of phase steps available for codifying the lens function. Our method permits to deal properly with the different arrival time of the light coming from different radial locations at the SLM plane. The segmentation of the pupil plane into subregions to measure wavefront aberrations was recently introduced in the field of high-resolution imaging in biological tissue [18]. In a second step, the lens function was codified onto the SLM, with the local phase modified in accordance with the results obtained at the sensing stage, and a laboratory experiment on the diffractive focusing of a 30 fs laser beam was carried out. Furthermore, our technique also opens the possibility of real-time tuning of femtosecond laser beams through the programmable nature of phase-only SLMs. Please note that emerging applications as compact pulse shaping based on a single SLM require aberration correction to obtain a high throughput in the output pulse [19–21].

2 Optical setup

We present a schematic of our experimental setup in Figure 1. An ultrashort laser source (FEMTOPOWER compact PRO from Femtolaser) emitted 30 fs light pulses at the central wavelength of 800 nm and repetition rate of 1 kHz. The pulsed beam was sent to a 4× all-mirror beam expander (BE) to better fit the active area of the SLM with an almost constant intensity beam. A pellicle beam splitter (BS) was inserted in the beam path. The transmitted beam was used to monitor the average power of the beam by means of a power meter (PM). The power was controlled using a variable attenuator consisting of a half-wave plate and a Glan-Thompson polarizer (not in the picture). The reflected beam impinged onto a liquid-crystal phase-only SLM (PLUTO-NIR from Holoeye) with 1920×1080 pixels and pixel pitch of 8 microns. The maximum peak intensity permitted to keep a well controlled SLM modulation is around 20 GW.cm^{-2} and the damage threshold is around 250 GW.cm^{-2} corresponding to 500 μJ and 7 mJ at 30 fs respectively for a complete use of the modulation area allowing further high field experiments.

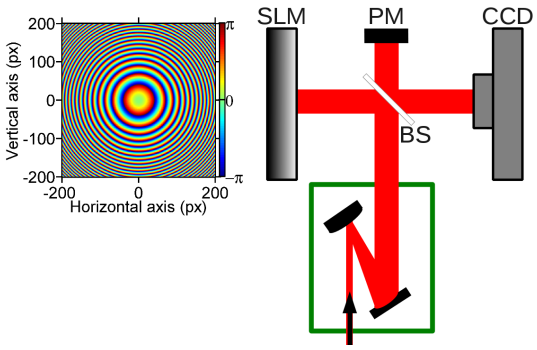

Fig. 1 Schematic of the optical setup. In the inset, phase transmission function encoded in the central 400×400 pixels of the SLM corresponding to a DL.

In order to focus the beam, we encoded a quadratic phase factor corresponding to a DL onto the SLM. Initially, we sent to the modulator the gray levels corresponding to the quadratic phase $\varphi(r)$ imparted by a lens of focal length f; i.e. $\varphi(r) = kr^2/(2f)$, with k the wave number and r the radial coordinate on the SLM pupil. In practice the SLM displays the phase wrapped in 2π steps. Focusing artifacts (such as multiple focal lengths and higher-order diffractions) due to the pixelated and the quantized nature of the SLM were taken into account. Quantization effects originate aliasing at the outer regions of the lens since the available number of pixels to codify each wrapped zone decreases with the distance to the center due to the squared dependence of the phase with the radial coordinate. In practical terms, this effect fixes the ultimate limit for the available minimum focal length, which is given by $f = kD\Delta r/(2\pi)$, with D the lens diameter and Δr the outermost zone width that must be longer than the pixel pitch. To overcome this limit, we encoded a DL of 130 mm of focal length for 800 nm in the SLM. The CMOS camera (Ueye UI-1540M - 8 bits) was located at the focal plane. The computed focal length can also be tuned so as not to saturate the camera and to obtain a reasonable spatial sampling.

Deviations from its ideal form were found and were attributed to unanticipated spatial phase inhomogeneities over the pulsed laser beam that can be described completely by the wave aberrations. It is defined as the difference between the perfect (plane) and the actual wavefront for every point at the pupil of the SLM for the mean wavelength. A perfect pulsed laser beam focuses to a circularly symmetric pattern. However, spatial phase inhomogeneities generate aberrations that produce a larger and, in general, asymmetric focal distribution. Wavefront aberrations were subsequently measured and corrected to achieve enhanced resolution and to generate high intensity in lensless pulsed beam focusing.

2.1 Wavefront sensing

To retrieve spatial phase inhomogeneities of the pulsed laser beam coming from the femtosecond system, the beam at the SLM plane was divided into N discrete zones that tile its whole active area and, thereby, was segmented into N beamlets individually controllable. Each zone corresponds to a circular ring whose inner, r_{in}, and outer radius, r_{out}, were chosen in such a way that the propagation time difference (PTD) for pulses originated at the two edges of the zone to the geometrical focus is smaller than the femtosecond pulse width. This propagation time difference can be calculated by the formula $(r_{out}^2 - r_{in}^2)/(2fc)$, where c is the speed of light [20,21]. In our experiment, we considered a PTD of 22 fs, i.e. the area of each ring was 5.32 mm^2. In addition we chose an approach based on ring overlapping. This means that one zone overlapped with the following by a distance equivalent to half of the PTD. With the above parameters the total number of rings employed was $N = 23$. When considering extremely short pulses, such as few-cycle pulses, this technique has technological limitations due to SLM dispersion on one hand and to the inhomogeneities of the spatial phase across the broad spectrum on the other.

We then applied the quadratic phase pattern corresponding to a DL with focal length 130 mm only to one of the zones. The remaining zones were driven with a phase pattern corresponding to a diverging lens that causes the associated beamlets generate negligible effect at the focus, rendering them effectively 'off'. We acquired an image at the focal plane using the sole remaining 'on' beamlet. An example of the SLM phase distribution corresponding to several ring-shaped zones used in the experiment can be found in figure 2 (*a-c*). To reduce the noise due to experimental fluctuations of the beam, we captured several images of the focal plane and averaged them. The focal irradiance measured with the camera for the corresponding rings are in figure 2 (*d-f*). Contribution of the innermost zone of the DL (ring 1) corresponds almost to the Airy pattern as can bee seen in figure 2 (*d*). However, as expected, the output pattern recorded

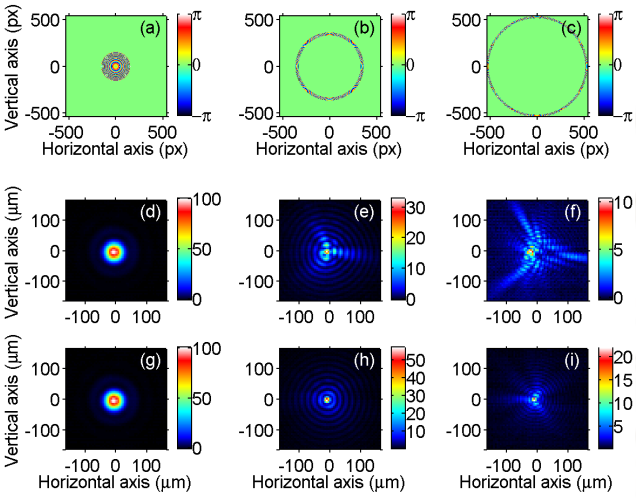

Fig. 2 (*a-c*) Phase transmission function encoded in the SLM corresponding to a DL with only one ring active (see text), in particular the 1$^{\text{st}}$, 10$^{\text{th}}$ and 23$^{\text{rd}}$ respectively. The measured irradiance in the focal plane for each ring without (*d-f*) and with (*g-i*) wavefront correction.

by the camera differs more from the ideal theoretical focal distribution of an homogeneous annulus for the outermost zones of the lens. This effect was attributed to the optical aberrations that have a strong dependence with the radial coordinate and prevents us to obtain a high-quality Airy spot when the whole area of the SLM is used to focus the beam. In figure 2 (*g-i*), we show results for the focal irradiance distribution generated by the above zones after wavefront sensing and compensation as is discussed throughout the rest of the paper. The key point in our pupil segmentation method is to take into account the broadband nature of short pulses to focus light nearly free of chromatic artifacts. As mentioned earlier, the broader the spectrum of the laser the higher the number of ring-shaped zones needed in the procedure. Following the generalized Huygens-Fresnel diffraction integral, the monochromatic depth of focus (DOF) for an annulus ring of a DL can be expressed by the formula $DOF \approx 1.76 f^2 \lambda_0/(r_{out}^2 - r_{in}^2)$. Whenever the DOF is longer than the longitudinal chromatic aberration of the focusing system we will be able to record with the camera structures close to the Airy pattern. Then, the retrieval process will be more accurate. In this way our method is more robust with respect to the presence of chromatic aberrations than other conventional methods. As mentioned earlier, the broader the spectrum of the laser the higher the number of ring-shaped zones. The ideal number of rings corresponds to that which allows to recover a structure close to the Airy pattern for each ring.

The next step is to find the azimuthal modulation in each of the rings that causes the observed pattern at focus. In order to do that, the angular variation is parameterized at a number of reference points uniformly

distributed at the SLM plane for subsequent spline interpolation. In our work we found that, for all the practical aberrations, 12 points are sufficient to recover the main information of the wavefront. As we deal with complex patterns, 24 independent parameters are required (12 for the amplitude and 12 for the phase). One of the 12 phase elements was fixed to remove the insensitive effect of a global shift in the absolute phase. To ensure that the fitting procedure is self-consistent, we also added the ring position and the width as free test parameters. The intensity distribution at focus derived from each set of intensities and phases was calculated through the Fourier Transform. The fit of the 25 parameters was obtained from a 2D least-squares fitting procedure where the searched target was the minimum Euclidean distance from the calculated to the experimental irradiance distribution at focus. The ring position and the width test parameters were checked in each reconstruction and were in agreement with the segmentation used in the experiment. With the remaining 23 parameters and by means of a spline interpolation we were able to obtain the retrieved intensity and phase as is shown in figure 3. In figure 3 (b) we illustrate the reconstructed output intensity from the retrieved amplitude and phase. The agreement between the measurement and the 2D fit is satisfactory.

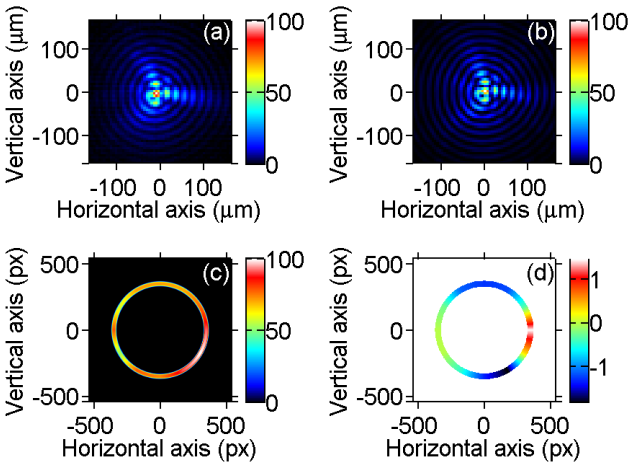

Fig. 3 Phase recovery procedure for a ring-shaped zone (10^{th} ring) over the SLM plane: (a) Experimental measurement of the focal irradiance; (b) Calculated irradiance distribution from the fitted phase; (c) retrieved intensity which for our experiment is almost uniform; (d) retrieved phase.

Next we repeated the previous procedure for the whole set of ring-shaped zones. To optimize the time required for the calculus, the final parameters obtained in one ring were used as the initial parameters for the next ring-shaped zone. The full phase over the SLM plane is generated through stacking the information obtained for each zone. The retrieved phase over the SLM pupil in our case is shown in figure 4 (a), where we have omitted the constant and the linear phase terms as they do not provide relevant information. These last terms correspond to cancel the Z_0^0, Z_1^{-1} and Z_1^1 Zernike coefficients (as shown in Fig. 4(c)). It has to be kept in mind that Z_0^0 term is the absolute spatial phase that cannot be detected with a linear detector, and $Z_1^{\pm 1}$ corresponds to a global displacement of the signal that can also be due to the vibration of the setup. In our example, few orders of Zernike polynomials are enough to correctly describe the spatial phase. We can see that numeric noise is more intense for the innermost zone. This is due to the fixed number of reference points used to sample the zones of the SLM plane, which are closer for this zone. To compare our results, we also calculated the aberrated

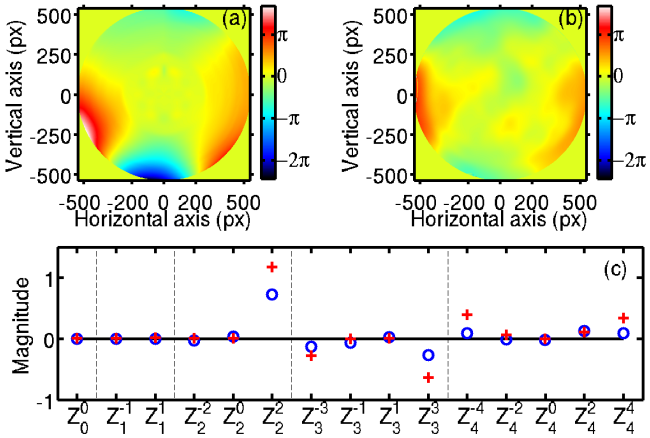

Fig. 4 Spatial phase reconstruction performed with the Fresnel phase retrieval (a) with annular lens array, and (b) with the full area. The Zernike coefficients [22] corresponding to the method shown in (a) (+) and method shown in (b) (∘) are displayed in (c).

wavefront with the Fresnel phase-retrieval method using the conventional iterative Fourier transform algorithm (IFTA) [12, 13]. We considered that the intensity over the SLM was constant and measured the focal irradiance pattern generated by the whole DL. In the iterative calculation, we analyzed the convergence of the algorithm by measuring the root mean square (rms) error between the image in the focal plane measured with the camera and the reconstructed image. Because the rms error of the intensity approaches an asymptotic value after iteration of the order of 100-300, the number of iterations was fixed at 300. The retrieved phase is shown in figure 4 (a). As will be seen below, for the border area of the pupil we have less information of the phase than the one obtained with the proposed annular lens array method.

2.2 Pulsed beam focusing

To provide a demonstration of the capabilities of our method, we designed an experiment for lensless focusing

of a femtosecond pulsed beam. To this end we simply used a SLM and no additional optics. Onto the SLM we encoded the quadratic phase factor corresponding to a DL, together with the phase that corresponds to the wavefront correction for our laser beam. Let us mention here that the drawback of the procedure (shared with other methods of diffractive correction of wavefront aberrations) is that the finite number of pixels of the SLM causes the efficiency of the encoded DLs to depend on the radial coordinate. This unwanted effect reduces the peak intensity of the pulses coming from the outer zones of the encoded DL. Satisfactorily, our method is well suited to measure the radial dependence, as the active area of the SLM is sampled through ring-shaped zones. For each ring-shaped zone, we evaluated the mean power that arrives to the focal plane and the values were normalized at its maximum value. In figure 5 (a), we show the dependence of the efficiency of our DL of 130 mm focal length with the ring number. Error bars correspond to the standard deviation, as several images per ring where used to calculate the corresponding efficiency. As expected from a theoretical point of view, focalization efficiency of the outermost ring is about 40% as the DL is encoded with only two phase levels [23].

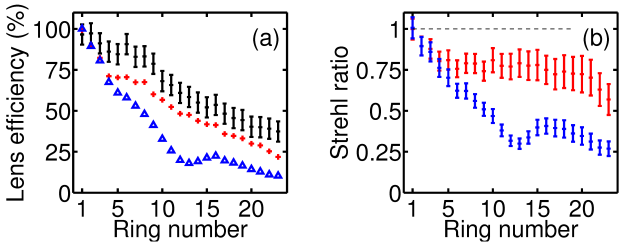

Fig. 5 (a) The diffraction efficiency of each of the rings used to segment the DL (see text for details) is presented by the black errorbar signal (+). The maximum peak intensity recorded in each images is shown for the uncompensated spatial phase (△) and the pupil segmentation compensation (+). The estimated Strehl ratio for each ring is then extracted in (b) for the uncompensated (+) and the compensated spatial phase (+)

Let us mention two different procedures to partially mitigate the radial drop of the diffraction efficiency. On the one hand, codification of DLs with a longer focal length helps, as the outermost zone width is higher. Unfortunately there are some applications where this is not an option. On the other hand, to guarantee a constant radial response it is possible to reduce the efficiency of the inner parts of the lens by controlling the design parameters through the maximum value of the wrapped phase [24]. In this way, the efficiency of the lens can be made constant over the whole radius at the expense of the reduction of the global energy derived to the main focal plane. This last solution has successfully been implemented in this configuration by our group in [19].

To quantify the improvement of the spatial phase compensation, we estimate the Strehl ratio for our 23 rings. If the spatial phase is flat, we may observe a constant ratio between the maximum of signal of each image and the image integral of signal for all the 23 rings (both shown in Fig.5 (a)). Since the first ring is a small disc, we can assume that the spatial phase is negligible, in this case the Strehl ratio is assumed to be 1. Hence, the Strehl ratios are evaluated for all the rings through a calibration with the central disc. This estimation is displayed in Fig.5 (b) for the measurement with and without corrections. The correction allows us to maintain a reasonable Strehl ratio for all the rings. It means that the spatial phase is almost completely removed. If the spatial phase is correctly removed for all the rings independently then the spatial phase can be deleted for the full spatial profile.

Finally let us compare in figure 6 the irradiance distribution in the focal plane of the encoded SLM in three different cases: (a) without wavefront correction, (b) with the wavefront correction provided by the Fresnel phase-retrieval method and (c) with the added phase obtained with our pupil segmentation method. It appears clear that the spatial phase has a strong influence on the focalization of the pulse. In figure 6 (a), the peak intensity is quite low (see colorbar) due to the fact that aberrations cause blurring of the focal spot. With the Fresnel phase-retrieval method, most of the problems have been corrected, the Strehl ratio has improved by about 36%, but the spatial compression is still not perfect. We attribute this fact to the poor quality of the image in figure 6 (a) used to retrieve the phase. The quantized levels of the camera and the broad spectrum of the laser pulse cause the blurring of the image, which results in a loss of resolution for the iterative method. Although the phase retrieval and pupil segmentation methods provide similar results with monochromatic illumination and high dynamic range cameras, we have found that in our experimental conditions, the pupil segmentation method provides better result because the fit with a limited number of parameters overcomes the limitation originated by the discrete intensity levels of the camera and the experimental noise. Therefore, pupil segmenta-

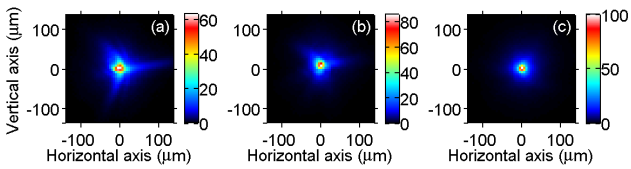

Fig. 6 Measurement of the intensity distribution of the full beam at the focal plane (a) without any correction of the spatial phase, (b) by using the Fresnel phase retrieval correction and (c) with the correction of the spatial phase presented in this article.

tion provides stronger focalization, with a Strehl ratio improved by about 60% compared with the uncorrected case. Furthermore, the circular symmetry of the output pattern is recovered, demonstrating that the SLM provides a convenient way to achieve maximum focusing power. This shows that annular segmentation into subregions is a well suited technique to measure with high accuracy polychromatic pulsed beams with low-dynamic range cameras.

3 Conclusion

In this paper, we present an innovative spatial phase retrieval method based on pupil segmentation. To implement our method only an SLM and a camera are needed. The pupil plane corresponds to the SLM, where a DL is encoded, and the output plane is the focal plane where the camera is placed. The pupil plane is decomposed into overlapped concentric rings and, at the same time, the corresponding irradiance for each ring is recorded with the camera. By means of a least square fitting procedure the phase and amplitude distribution of the input beam over the SLM plane was retrieved. In our experiment the amplitude was almost flat and the phase was compared with the one obtained with the Fresnel phase retrieval method. We found that our proposal provides more accurate results. To test our method we did an experiment based on lensless focusing a 30 fs femtosecond laser beam. To increase the quality of the focal spot aberrations were corrected. The complex conjugate phase of the retrieved phase was encoded onto the SLM together with the DL. We observed that the spatial quality and intensity of the focal spot obtained at the focal plane are higher when compared with the conventional Fresnel phase retrieval method. This was attributed to pupil segmentation that allows to overcome the limitations associated with the poor dynamic range of conventional cameras. This advantage is even crucial with polychromatic coherent beams such as the 30 fs pulse employed in the present experiment. In this case, we demonstrated that pupil segmentation is a well suited technique to overcome the additional blurring associated with chromatic aberrations in the Fresnel phase-retrieval method. Work is in progress to reduce the number of acquisitions, keeping the same dynamic range, to make the technique well suited also for low repetition rate lasers. The adaptation of the Fresnel phase-retrieval method to the pupil segmentation technique will be seen elsewhere.

Acknowledgements This work was supported by the Spanish Ministerio de Economia y Competitividad (MINECO) and FEDER through the projects FIS2010-15746, SAUUL (CSD2007-00013) and CTQ2008-02578. Also, financial support from the Generalitat Valenciana through project PROMETEO/2012/021 Fundació Caixa-Castelló through project P11B2010-26 and European network ITN FASTQUAST (PITN-GA-2008-214962) is acknowledged. The authors are grateful to the Serveis Centrals d'Intrumentació Científica of the Universitat Jaume I for the use of the femtosecond laser.

References

1. K. Akaoka, S. Harayama, K. Tei, Y. Maruyama, and T. Arisawa, Proc. SPIE **3265,** (1998) 219.
2. B. Schäfer, K. Mann, G. Marowsky, C. P. Hauri, J. Biegert, and U. Keller, Proc. SPIE **5918,** 59180P
3. T. A. Planchon, J.-P. Rousseau, F. Burgy, G. Chériaux, and J.-P. Chambaret, Opt. Commun. **252,** (2005) 222.
4. S.-W. Bahk, P. Rousseau, T. A. Planchon, V. Chvykov, G. Kalintchenko, A. Maksimchuk, G. A. Mourou, and V. Yanovsky, Opt. Lett. **29,** (2004) 2837.
5. V. Yanovsky, V. Chvykov, G. Kalinchenko, P. Rousseau, T. Planchon, T. Matsuoka, A. Maksimchuk, J. Nees, G. Cheriaux, G. Mourou, and K. Krushelnick, Opt. Express **16,** (2008) 2109.
6. Wattellier, J. Fuchs, J. P. Zou, K. Abdeli, C. Haefner, and H. Pépin, Rev. Sci. Inst. **75,** (2004) 5186.
7. A. Ruiz de la Cruz, A. Ferrer, W. Gaweld, D. Puerto, M. Galván Sosa, J. Siegel, and J. Solis, Opt. Express **17,** (2009) 20853.
8. J. M. Bueno, B. Vohnsen, L. Roso, and P. Artal, Appl. Opt. **49,** (2009) 770.
9. J.-C. Chanteloup, F. Druon, M. Nantel, A. Maksimchuk, and G. Mourou, Opt. Lett. **23,** (1998) 621.
10. R. Borrego-Varillas, C. Romero, J. R. Vázquez de Aldana, J. M. Bueno, and L. Roso, Opt. Express **19,** (2011) 22851.
11. J. R. Fienup and C. C. Wackerman, Opt. Lett. **3**, 2729 (1978).
12. S. Matsuoka and K. Yamakawa, J. Opt. Soc. Am. B **17,** (2000) 663.
13. T. M. Jeong, C. M. Kim, D.-K. Ko, and J. Leet, J. Opt. Soc. Kor. **12,** (2008) 186.
14. J. L. Martínez, I. Moreno, and E. Ahouzi, Eur. J. Phys. **27,** (2006) 1221.
15. A. Márquez, C. Iemmi, J. Campos, and M. J. Yzuel, Opt. Lett. **31,** (2006) 392.
16. J. Arines, V. Durán, Z. Jaroszewicz, J. Ares, E. Tajahuerce, P. Prado, J. Lancis, S. Bará, and V. Climent, Opt. Express **15,** (2007) 15287.
17. E. Carcolé, J. Campos, and S. Bosch, Appl. Opt. **33,** (1994) 162.
18. N. Ji, D. E. Milkie, and E. Betzig, Nature Methods **7,** (2010) 141.
19. O. Mendoza-Yero, V. Loriot, J.Prez-Vizcano, G. Mnguez-Vega, J. Lancis, R. de Nalda, L. Baares, Opt. Letts. 5067-5069 (2012)
20. G. Mínguez-Vega, O. Mendoza-Yero, J. Lancis, R. Gisbert, and P. Andrés, Opt. Express. **16,** (2008) 16993.
21. V. Loriot, O. Mendoza-Yero, G. Minguez-Vega, L. Bañares and R. de Nalda, IEEE Photon. Technol. Lett. **24** 273-275 (2012).
22. American National Standard for Ophthalmics. ANSI® Z80.28-2009, Annex 6.
23. S. Sinzinger and J. Jahns, *Microoptics* (Wiley VCH, Weinheim, Germany, 2003).
24. V. Moreno, J. F. Román, and J. R. Salgueiro, Am. J. Phys. **65,** (1997) 556.